ACS Energy LETTERS

http://pubs.acs.org/journal/aelccp
Letter

Direct Microscale Observation of Additive-Triggered Reduction in Tin Halide Perovskites

Robert J. E. Westbrook,* Margherita Taddei, Jesús Sanchez-Diaz, Tehmina Mushtaq, Rafael S Sánchez, Luis Lanzetta, Rajiv Giridharagopal, David S. Ginger, and Iván Mora-Seró*

Cite This: https://doi.org/10.1021/acsenergylett.6c01751
Read Online

ABSTRACT: We investigate the nanoscale function of additives used for tin-containing perovskites, using the archetypal $FASnI_3$ (FA = formamidinium). First, we find that the addition of sodium borohydride ($NaBH_4$) is inhomogeneous, with 200–500 nm aggregates forming on the $FASnI_3$ surface. The inhomogeneous distribution of $NaBH_4$ leads to a relatively small (~1% of the film) amount of reduced perovskite, but the macroscopic properties are dominated by the overwhelming space without any treatment. Upon illumination, more aggregate regions (~13%) become activated due to reduction of photogenerated I_2. On the other hand, when we combine $NaBH_4$ with dipropylammonium iodide (DipI) passivation and illuminate, we observe a much more homogeneous activation effect, which we attribute to denser coverage of $NaBH_4$. We find that the iodine content in $FASnI_3$ films treated with $NaBH_4$ and DipI is 64% less than in those treated with $NaBH_4$ alone. These results underline that the microscale configuration of different additives in tin perovskites is deeply interconnected and it is essential to uncover their chemical reactivity.

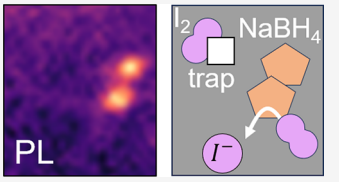

Tin halide perovskite semiconductors ($ASnX_3$) hold promise for broad application in optoelectronics. In photovoltaics, the field has mostly focused on $FASnI_3$ (FA = formamidinium) due to the superior stability of the FA cation (relative to e.g., methylammonium) and because the bandgap of this composition approaches the maximum of the solar spectrum, thus leading to high theoretical power conversion efficiency (PCE).[1,2] Moreover, an understanding of Sn chemistry is essential for the development of all-perovskite tandem solar cells, which have far surpassed the record efficiency of single junction perovskites and could approach 40% power conversion efficiency.[3−5] However, the PCE of photovoltaics based on $FASnI_3$ is far from that achieved in $APbX_3$ perovskites due to severe open-circuit voltage (V_{OC}) and short-circuit current (J_{SC}) losses.[6] These losses arise due to the lower oxidation potential of the Sn(II)/Sn(IV) redox couple (oxidized even in air-free conditions by dimethylsulfoxide in the precursor solution),[7] leading to electron trapping via Sn(IV) traps at the surface and higher recombination rates in the bulk associated with excessive *p*-type doping.[8−14]

Researchers have pioneered passivating and reducing additives to tame this complex redox chemistry. Lewis bases like guanidinium thiocyanate or dipropylammonium iodide (DipI), which strongly coordinate with Sn(II) in the lattice, have been used to simultaneously slow crystallization and limit the amount of Sn(IV) formed initially.[15−19] SnF_2 has been developed to sequester Sn(IV) into SnF_4, which would otherwise serve as an electron trap (eq 1).[8] Moreover, surface Sn(IV) can undergo photolysis to yield SnI_2 and I_2 (eq 2),[16] a process that removes Sn(IV)-related traps due to photoreduction to Sn(II). However, the presence of I_2 also destabilizes the system because it can react with the perovskite to form further Sn(IV)I_4 traps (eq 3).[20−22] More recently, sodium borohydride ($NaBH_4$) has been used to provide additional conversion of Sn(IV) to Sn(II), as well as reduce I_2 to I^-, which can then be incorporated back into the lattice (eq 4).[16,23−25] Considering an apparent $NaBH_4$ redox potential of −0.54 V in DMF,[26] both the I_2/I^- (+0.54 V vs standard hydrogen electrode [SHE])[16] and Sn^{4+}/Sn^{2+} (E_o^{red} = +0.15 V vs SHE)[16] reduction reactions have large overall cell potentials (E_{cell}^0) of +1.08 V and +0.69 V, respectively. When computed via the Gibbs equation, these high voltages yield negative ΔG values of −208 kJ mol^{-1} and −133 kJ mol^{-1}, respectively, favoring the spontaneous formation of I^- and Sn^{2+}.

$$SnI_4 + SnF_2 \rightarrow SnI_2 + SnF_4 \quad (1)$$

$$SnI_4 + h\nu \rightarrow SnI_2 + I_2 \quad (2)$$

$$ASnI_3 + I_2 \rightarrow SnI_4 + AI \quad (3)$$

$$2NaBH_4 + I_2 \rightarrow 2NaI + 2BH_3 + H_2 \quad (4)$$

Despite these great advances in the understanding of additives to control self-doping in $FASnI_3$, almost all work has been done

Received: June 10, 2026
Revised: July 22, 2026
Accepted: August 18, 2026

with bulk techniques, which cannot resolve the nano- and microscale heterogeneities that result from solution processing. Since metal halide perovskites are highly heterogeneous materials, understanding the microscale effects of additives—in isolation and in synergy—is essential for informed device fabrication.[10,27−29]

In this study, we address this gap in the understanding of tin-halide perovskite-additive interactions by applying multimodal microscopy to $FASnI_3$ films with different additives. We find that $NaBH_4$ organizes in aggregates on the $FASnI_3$ surface, which localizes the reduction effect to the immediate vicinity of these features. Upon illumination, we find that more $NaBH_4$ sites begin to reduce I_2. Moreover, we find that the additional application of dipropylammonium iodide (DipI) is essential for homogeneous distribution of the otherwise clustered $NaBH_4$, leading to a more homogeneous reduction effect.

We spin-coated $FASnI_3$ films with different precursor preparations: (i) $FASnI_3$ without $NaBH_4$ and DipI additives (hereafter $FASnI_3$); (ii) $FASnI_3$ with $NaBH_4$ ($FASnI_3$ + $NaBH_4$); (iii) $FASnI_3$ with DipI ($FASnI_3$ + DipI); and (iv) $FASnI_3$ with both $NaBH_4$ and DipI ($FASnI_3$ + $NaBH_4$ + DipI). We note that in all cases, including $FASnI_3$, we used SnF_2 as an additional additive to limit the formation of tin vacancies (V_{Sn}). We recorded atomic force microscopy and hyperspectral photoluminescence (PL) images of the $FASnI_3$ samples with different additives to obtain a microscale picture of additive-induced reduction in each case. The hyperspectral PL technique enables simultaneous characterization of spatial and spectral heterogeneity in PL intensity with sub-micron resolution.[28−31] We provide details of our film processing and characterization in the Supporting Information.

In Figure 1a,b, we present AFM topography and phase images of a $FASnI_3$ film treated with $NaBH_4$. The film topography is characterized by the expected perovskite morphology (rough morphological grain size 500–1000 nm), as well as an additional contribution from apparent non-perovskite aggregates (size < 500 nm) with a density of 0.5% (Figure S1). We suspect these to be $NaBH_4$ aggregates given that they (i) lie on the surface of the perovskite consistent with our previous XPS work,[16] and (ii) they only appear in $NaBH_4$-treated samples with a distinct shape and size to the SnF_2/SnF_4 aggregates observed in $FASnI_3$ films (Figures S2 and S3).

In Figure 1c,d, we show photoluminescence intensity and peak energy maps of the same region as measured with hyperspectral PL. Strikingly, the three regions underneath $NaBH_4$ aggregates have brighter (Figure 1b) and red-shifted (Figure 1c) PL, consistent with a localized reduction effect, which we attribute to reduction of Sn(IV) and/or I_2.[10] We discuss other possible explanations for the PL brightening and red-shift phenomenon in Note S1 and Figure S4. This situation is sub-optimal because the majority of the film is not being impacted by the additive, maintaining high nonradiative rates that ultimately limit performance. We show a correlation between the AFM phase and PL intensity images over a larger 50 × 50 μm region in Figure S5.

We next investigated the effect of $NaBH_4$ and DipI during illumination, to elucidate the role of the photochemistry outlined in eqs 2–4 on the different samples. We chose 3 days of AM1.5 illumination because this was the timeframe over which we observed maximum Sn(II)/Sn(IV) and I^-/I_2 ratios in our previous work.[16] To do this, we (i) scratched a fiducial box around a region of interest with an AFM tip, (ii) measured an "initial" PL microscopy image, (iii) aged the samples under AM1.5 illumination for three days, and (iv) measured a "3 days" PL microscopy image of the same region as measured in (i). We first analyzed the $FASnI_3$ + $NaBH_4$ films. In Figure 2a and b we show PL microscopy images of a $FASnI_3$ + $NaBH_4$ film at 860 nm initially and after 3 days of illumination. The initial PL microscopy image consists of bright spots, which are likely underneath $NaBH_4$ aggregates as shown earlier. Upon illumination, we observe that further bright spots appear (in addition to the original ones, which are maintained, see Figure S6). We also notice that the contrast between the bright spots and the background becomes less pronounced after light soaking. This is

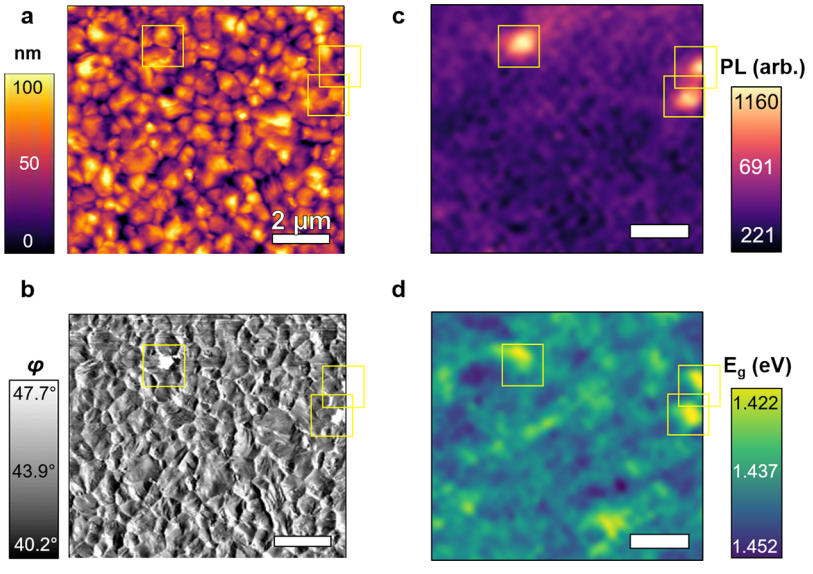

Figure 1. $NaBH_4$ aggregates impose a localized reduction effect. (a) Atomic force microscopy (AFM) topography image of a $FASnI_3$ film treated with $NaBH_4$. (b) AFM phase image of the same region of the $FASnI_3$ film treated with $NaBH_4$. (c) Photoluminescence (PL) intensity image at 860 nm of the same region in (a) and (b). (d) Peak emission energy map extracted from the hyperspectral PL data. We highlight the locations of $NaBH_4$ aggregates with yellow boxes. The scalebars in all panels are 2 μm.

https://doi.org/10.1021/acsenergylett.6c01751
ACS Energy Lett. XXXX, XXX, XXX−XXX

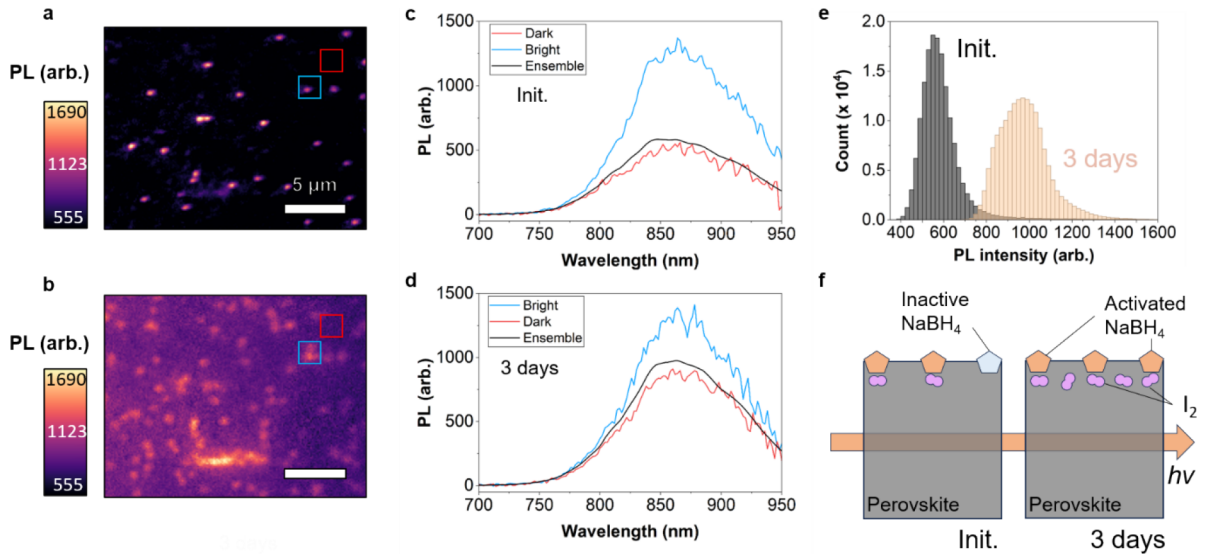

Figure 2. Reducing effect of $NaBH_4$ additive spreads out under illumination. (a, b) Correlated PL intensity images at 860 nm initially (a) and after 3 days of illumination at 1 sun (b). The scalebars in both images are 5 μm. (c, d) Photoluminescence spectra extracted from blue and red boxes in (a, b), before (c) and after (d) illumination at 1 sun for 3 days. (e) Histogram data for the PL intensity at each pixel in the hyperspectral images. (f) Illustration of propagation of bright spots in PL images—initially, only those regions underneath $NaBH_4$ aggregates with a considerable amount of I_2 in the immediate vicinity are activated; later, additional aggregates are activated as more I_2 evolves at the film surface. Photobrightening is inhomogeneous because it is limited to regions underneath the $NaBH_4$ aggregates.

further demonstrated by the point spectra in Figure 2c,d, which relate to the red and blue boxes in (a) and (b). Initially, the PL spectrum associated with one of the bright spots contained within the blue box is 2-3 times larger than the dark region in the red box. Upon illumination, the PL intensity of the bright spot within the blue box is the same, but the PL in the red box has increased by ∼1.5X to within 20% of the blue box.

Importantly, the ensemble PL spectrum (black, Figure 2c,d) tends to be dominated by the darker regions (red) and thus it is also important to look at the extent of activation across the entire image. The histogram data in Figure 2e helps realize this view of photobrightening in $FASnI_3$ + $NaBH_4$ films. The initial film (black) is dominated by emission at ∼600 counts with a small tail of emission above 1000 counts associated with the bright spots, corresponding to an estimated 1.3% of the image (Figure S7). The film after 3 days of light soaking (orange) is dominated by emission at ∼1000 counts with a larger tail of emission above 1000 counts, corresponding to an estimated 13.2% of the image (Figure S8). Thus, although light soaking has spread out the reducing effect of the $NaBH_4$ to a degree, much of the film (>85%) has not experienced any effect. This is manifest in the shape of the histogram for the film after light soaking, which is strikingly non-Gaussian, suggesting at least two distinct groups contributing to PL emission (i.e., bright spots under aggregates and darker spots elsewhere). In Figure 2f we illustrate the likely mechanism underpinning this effect: initially, only a small subset of perovskite/$NaBH_4$ regions have a significant I_2 density, inducing the redox chemistry that reduces the local nonradiative rates ("activation"). During illumination, more I_2 is generated at the surface due to photolysis of SnI_4, allowing additional perovskite/$NaBH_4$ sites to become activated.

Secondly, we investigated the effect of $NaBH_4$ + DipI addition. In Figure 3a,b we show PL microscopy images of a $FASnI_3$ + $NaBH_4$ + DipI film at 860 nm initially and after 3 days of illumination (corresponding AFM images in Figure S9). As with $FASnI_3$ + $NaBH_4$, the initial PL microscopy image consists of darker regions and bright spots, which are likely $NaBH_4$ aggregates with a significant local I_2 density. Upon illumination, additional bright spots appear at a higher density than with the $FASnI_3$ + $NaBH_4$ film. Turning to the point spectra in Figure 3c,d, we again observe strong heterogeneity in the initial case, with a bright spot having 2 times higher PL intensity than a dark region. The key takeaway from the $FASnI_3$ + $NaBH_4$ + DipI film is clearly highlighted in the histogram in Figure 3e. The initial behavior is strikingly similar to the $FASnI_3$ + $NaBH_4$ film case, where the image is dominated by "dark" pixels at ∼600 counts with a small number of pixels at higher counts associated with the bright spots (1.9 %, Figure S10). However, upon illumination, most of the pixels become activated ("bright") to >1100 counts (88.9%, Figure S11). In contrast to the $FASnI_3$ + $NaBH_4$ films, the histogram for the $FASnI_3$ + $NaBH_4$ + DipI film after 3 days of light soaking has a more Gaussian shape than for $FASnI_3$ + $NaBH_4$, suggesting one main grouping of emitting states.

We also investigated $FASnI_3$ + DipI films, which we show in Figures S12 and S13. A key difference with these films is that the grain size is larger than in the other films, which we expect is due to the role of DipI as a passivator and crystallization modifier.[16] We expect the resulting $FASnI_3$ + DipI films to have a lower surface/volume ratio, reducing the Sn(IV) content in the film and thus reducing nonradiative recombination, leading to the higher initial photoluminescence intensity. Upon illumination, we observe an overall 2X increase in PL intensity, but the original spatial PL distribution remains similar. We attribute this to blanket photolysis of Sn(IV). However, given that there is no $NaBH_4$ present, we expect the build up of I_2 to strongly impact the stability of $FASnI_3$ + DipI films, as shown in previous work.[16]

https://doi.org/10.1021/acsenergylett.6c01751
ACS Energy Lett. XXXX, XXX, XXX–XXX

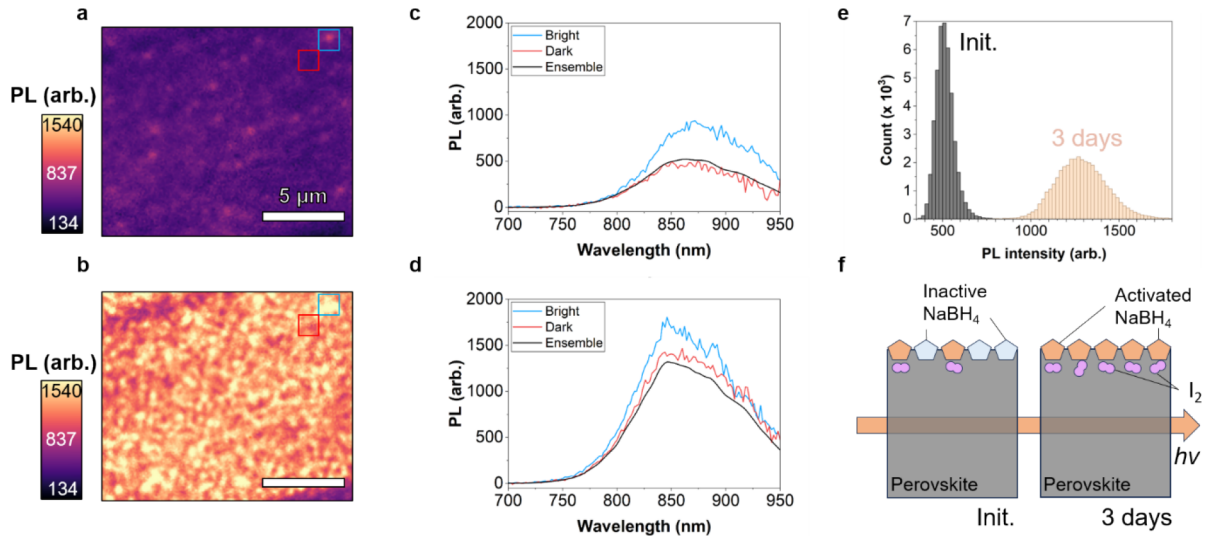

Figure 3. Distribution of $NaBH_4$ is more homogeneous when combined with DipI. (a, b) PL intensity images initially (a) and after 3 days of illumination at 1 sun (b) for a $FASnI_3$ + DipI + $NaBH_4$ film. (c, d) Photoluminescence spectra extracted from blue and red boxes before (c) and after (d) illumination at 1 sun for 3 days. (e) Histogram data for the PL intensity at each pixel in the hyperspectral images. (f) Illustration of propagation of bright spots in PL images – initially, only those regions with a considerable amount of I_2 in the immediate vicinity of $NaBH_4$ aggregates are activated; later, additional aggregates are activated as more I_2 evolves from the bulk film. Photobrightening is more homogeneous because the $NaBH_4$ is well distributed.

Figures S2 and S3 show correlated atomic force microscopy (AFM) and PL intensity maps for $FASnI_3$ without $NaBH_4$ or DipI additives. Figure S2c shows that the spatial PL in $FASnI_3$ is mostly dim with some isolated, higher intensity regions. Moreover, the point spectra in Figure S2d demonstrate that the dim regions are strongly blue-shifted (peak ~ 800 nm) with respect to the brighter regions (~870 nm). In our previous work, we demonstrated that this peak emission shift is due to band-filling effects that arise from self-doping.[10] Given that the spatial profile of the red-shifted (less-doped) regions

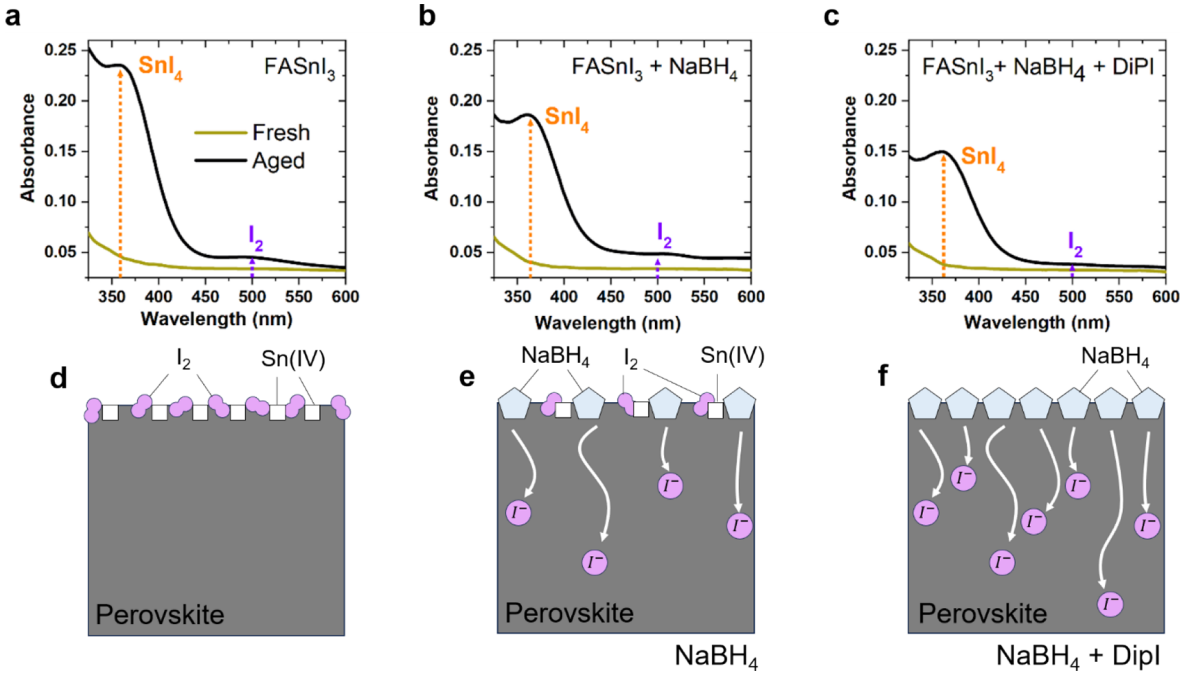

Figure 4. Better distribution of $NaBH_4$ promotes more I_2 reduction. (a–c) UV–vis absorption data of solutions made from fresh (green) and aged (black) $FASnI_3$ (a), $FASnI_3$ + $NaBH_4$ (b), and $FASnI_3$ + $NaBH_4$ + DipI (c) films. (d–f) Illustration of likely PL enhancement mechanism. Without $NaBH_4$ (d), I_2 evolves freely at the surface leading to the formation of additional Sn(IV) traps and nonradiative recombination. In the case of $FASnI_3$ + $NaBH_4$ (e), the density of $NaBH_4$ aggregates on the surface is not sufficient to convert all I_2 to I^-. For $FASnI_3$ + $NaBH_4$ + DipI (f), there is a higher density of $NaBH_4$ aggregates on the surface, which allows for more efficient conversion of I_2 to I^-.

https://doi.org/10.1021/acsenergylett.6c01751
ACS Energy Lett. XXXX, XXX, XXX–XXX

matches well with topological features above the surface of the perovskite film identified in atomic force microscopy (AFM) (Figure S2a,b), these regions are likely underneath aggregates of SnF_4. In Figure S3, we show the PL map and point spectra of the same region after 3 days of AM 1.5 illumination at 1 Sun, demonstrating that the spatial PL profile is mostly unchanged over this period.

Given that the differences under illumination should be governed by eqs 2–4 in the introduction (and thus the I_2 and Sn chemistry), we investigated I_2 generation in the films after illumination with UV–vis absorption spectroscopy. For this, we sealed perovskite samples inside vessels under inert atmosphere, and extracted degradation products via washing with toluene after 3 days of ageing under AM 1.5G illumination. As shown in Figure 4a–c, we identify two absorption bands characteristic of SnI_4 and I_2 at ∼360 nm and ∼500 nm, respectively.[20] Relative to $FASnI_3$, the $FASnI_3$ + $NaBH_4$ and $FASnI_3$ + $NaBH_4$ + DipI films generate ∼53% and ∼70% less I_2, respectively (further details in Figure S14).

Based on the results of our study, we provide the associated mechanism for the respective I_2 content in the different Sn perovskite films in Figure 4d–f. In the absence of any $NaBH_4$, I_2 is free to build up at the surface and can react with SnI_2 to form SnI_4, an electron trap (Figure 4d).[20,21] For $FASnI_3$ + $NaBH_4$, there is limited reduction of I_2 to I^- in the immediate vicinity of $NaBH_4$, resulting in a lower yield of I_2, and thus a lower signature of SnI_4 (Figure 4e). However, there is even less I_2 produced in the case of $FASnI_3$ + $NaBH_4$ + DipI because the distribution of $NaBH_4$ is more homogeneous, leading to more I_2 reduction events and the lowest SnI_4 content of all the studied films (Figure 4f). We propose that this improved distribution of $NaBH_4$ may stem from interaction with DipI ions in solution, or the slower crystallization in the presence of DipI.[15] Furthermore, we have shown that the larger crystal size in $FASnI_3$ + DipI is an important factor limiting nonradiative recombination in Sn perovskites. Thus, we expect that further improvements in Sn perovskite optoelectronic properties are possible by optimizing the combination of passivating (e.g., DipI) and reducing (e.g., $NaBH_4$) additives synergically to produce films with a low defect density and a homogeneous distribution of $NaBH_4$ and other additives. Our previous work shows that the combination of the passivating (DipI) and reducing ($NaBH_4$) additives is also critical to long-term stability because the buildup of I_2 at the surface cannot be controlled without $NaBH_4$.[16] Thus, the better distribution of $NaBH_4$ with DipI leads to a more homogeneous I_2 reduction effect, which improves long-term stability.

In summary, our findings demonstrate that the nanoscale action of additives such as DipI and $NaBH_4$ is critical for effective management of the dopant and defect densities in tin halide perovskites, highlighting the synergistic effect of passivating and reducing additives. In particular, we find that, although there are isolated regions of effective reduction when $NaBH_4$ is used alone, the bulk PL properties are still dominated by the dark regions far from the $NaBH_4$. When $NaBH_4$ is used in conjunction with DipI, we observe a more homogeneous reduction effect, which is more beneficial for the macroscopic optoelectronic quality of the film. Our work shows that the microscale organization of additives needs to be considered to rationalize and optimize the bulk chemistry in these materials, and we expect further optimization to be possible with correlative microscopy approaches.

■ ASSOCIATED CONTENT

Supporting Information

The Supporting Information is available free of charge at https://pubs.acs.org/doi/10.1021/acsenergylett.6c01751.

Aggregate masking with atomic force microscopy (AFM); correlative microscopy of $FASnI_3$ film without additives; bulk XRD patterns of $FASnI_3$ and $FASnI_3$ + DipI; correlative microscopy of $FASnI_3$ + $NaBH_4$ film over a larger region; correlative microscopy of $FASnI_3$ + $NaBH_4$ films with original bright spots highlighted; demonstration of mask applied to determine percentage of bright spots in $FASnI_3$ + $NaBH_4$; correlative microscopy of $FASnI_3$ + $NaBH_4$ + DipI film; demonstration of mask applied to determine percentage of bright spots in $FASnI_3$ + $NaBH_4$ + DipI; correlative microscopy of $FASnI_3$ + DipI (DOCX)

■ AUTHOR INFORMATION

Corresponding Authors

Robert J. E. Westbrook – *Department of Chemistry, University of Washington, Seattle, Washington 98195-1700, United States;* orcid.org/0000-0002-1203-0712; Email: rw794@cam.ac.uk

Iván Mora-Seró – *Institute of Advanced Materials (INAM), Universitat Jaume I, Av. Sos Baynat, s/n, Castellón 12071, Spain;* orcid.org/0000-0003-2508-0994; Email: sero@uji.es

Authors

Margherita Taddei – *Department of Chemistry, University of Washington, Seattle, Washington 98195-1700, United States;* orcid.org/0000-0003-4122-8418

Jesús Sanchez-Diaz – *Institute of Advanced Materials (INAM), Universitat Jaume I, Av. Sos Baynat, s/n, Castellón 12071, Spain*

Tehmina Mushtaq – *Institute of Advanced Materials (INAM), Universitat Jaume I, Av. Sos Baynat, s/n, Castellón 12071, Spain*

Rafael S Sánchez – *Institute of Advanced Materials (INAM), Universitat Jaume I, Av. Sos Baynat, s/n, Castellón 12071, Spain;* orcid.org/0000-0001-8948-6120

Luis Lanzetta – *Institute of Advanced Materials (INAM), Universitat Jaume I, Av. Sos Baynat, s/n, Castellón 12071, Spain;* orcid.org/0000-0001-5591-1010

Rajiv Giridharagopal – *Department of Chemistry, University of Washington, Seattle, Washington 98195-1700, United States;* orcid.org/0000-0001-6076-852X

David S. Ginger – *Department of Chemistry, University of Washington, Seattle, Washington 98195-1700, United States;* orcid.org/0000-0002-9759-5447

Complete contact information is available at: https://pubs.acs.org/doi/10.1021/acsenergylett.6c01751

Notes

The authors declare no competing financial interest.

■ ACKNOWLEDGMENTS

R.W., M.T., and D.S.G., were primarily supported by the U.S. National Science Foundation through the UW Molecular

Engineering Materials Center (MEM-C), a Materials Research Science and Engineering Center (DMR-1719797). R.W. also acknowledges support from the Momental Foundation via the Mistletoe Research Fellowship. This work is partially funded by the Ministerio de Ciencia e Innovación of the Spanish Government by the project PLEDs, PID2022-140090OB-C21/AEI/10.13039/501100011033/FEDER. R.G. acknowledges the support of the U.S. Department of Energy, Office of Basic Energy Sciences, Division of Materials Sciences and Engineering under Award DE-SC0013957 for supporting the AFM work. L.L. acknowledges support from the European Union's Horizon Europe research and innovation programme under the Marie Skłodowska-Curie Actions Postdoctoral Fellowship (grant agreement No. 101153098).

■ REFERENCES

(1) Nasti, G.; Abate, A. Tin Halide Perovskite ($ASnX_3$) Solar Cells: A Comprehensive Guide toward the Highest Power Conversion Efficiency. *Adv. Energy Mater.* **2020**, *10* (13), No. 1902467.

(2) Pitaro, M.; Tekelenburg, E. K.; Shao, S.; Loi, M. A. Tin Halide Perovskites: From Fundamental Properties to Solar Cells. *Adv. Mater.* **2022**, *34* (1), No. 2105844.

(3) Chen, B.; Yu, Z.; Onno, A.; Yu, Z.; Chen, S.; Wang, J.; Holman, Z. C.; Huang, J. Bifacial All-Perovskite Tandem Solar Cells. *Sci. Adv* **2022**, *8*, No. eadd0377.

(4) Lin, R.; Xu, J.; Wei, M.; Wang, Y.; Qin, Z.; Liu, Z.; Wu, J.; Xiao, K.; Chen, B.; Park, S. M.; Chen, G.; Atapattu, H. R.; Graham, K. R.; Xu, J.; Zhu, J.; Li, L.; Zhang, C.; Sargent, E. H.; Tan, H. All-Perovskite Tandem Solar Cells with Improved Grain Surface Passivation. *Nature* **2022**, *603* (7899), 73−78.

(5) Lin, R.; Wang, Y.; Lu, Q.; Tang, B.; Li, J.; Gao, H.; Gao, Y.; Li, H.; Ding, C.; Wen, J.; Wu, P.; Liu, C.; Zhao, S.; Xiao, K.; Liu, Z.; Ma, C.; Deng, Y.; Li, L.; Fan, F.; Tan, H. All-Perovskite Tandem Solar Cells with 3D/3D Bilayer Perovskite Heterojunction. *Nature* **2023**, *620*, 994−1000.

(6) Li, T.; Luo, X.; Wang, P.; Li, Z.; Li, Y.; Huang, J.; Jin, Z.; Yang, Y.; Li, B.; Zhang, W.; Lin, S.; Rui, Y.; Wang, H.; Zhang, Q.; Zhan, Y.; Xu, B.; Liang, J.; Qi, Y. Tin-Based Perovskite Solar Cells with a Homogeneous Buried Interface. *Nature* **2025**, *648* (8092), 84−90.

(7) Pascual, J.; Nasti, G.; Aldamasy, M. H.; Smith, J. A.; Flatken, M.; Phung, N.; Di Girolamo, D.; Turren-Cruz, S. H.; Li, M.; Dallmann, A.; Avolio, R.; Abate, A. Origin of Sn(Ii) Oxidation in Tin Halide Perovskites. *Mater. Adv.* **2020**, *1* (5), 1066−1070.

(8) Dey, K.; Roose, B.; Stranks, S. D. Optoelectronic Properties of Low-Bandgap Halide Perovskites for Solar Cell Applications. *Adv. Mater.* **2021**, *33* (40), No. 2102300.

(9) Ricciarelli, D.; Meggiolaro, D.; Ambrosio, F.; De Angelis, F. Instability of Tin Iodide Perovskites: Bulk p-Doping versus Surface Tin Oxidation. *ACS Energy Lett.* **2020**, *5* (9), 2787−2795.

(10) Westbrook, R. J. E.; Taddei, M.; Giridharagopal, R.; Jiang, M.; Gallagher, S. M.; Guye, K. N.; Warga, A. I.; Haque, S. A.; Ginger, D. S. Local Background Hole Density Drives Nonradiative Recombination in Tin Halide Perovskites. *ACS Energy Lett.* **2024**, *9* (2), 732−739.

(11) Milot, R. L.; Klug, M. T.; Davies, C. L.; Wang, Z.; Kraus, H.; Snaith, H. J.; Johnston, M. B.; Herz, L. M. The Effects of Doping Density and Temperature on the Optoelectronic Properties of Formamidinium Tin Triiodide Thin Films. *Adv. Mater.* **2018**, *30* (44), No. 1804506.

(12) Kahmann, S.; Shao, S.; Loi, M. A. Cooling, Scattering, and Recombination—The Role of the Material Quality for the Physics of Tin Halide Perovskites. *Adv. Funct. Mater.* **2019**, *29* (35), No. 1902963.

(13) Milot, R. L.; Eperon, G. E.; Green, T.; Snaith, H. J.; Johnston, M. B.; Herz, L. M. Radiative Monomolecular Recombination Boosts Amplified Spontaneous Emission in $HC(NH_2)_2SnI_3$ Perovskite Films. *J. Phys. Chem. Lett.* **2016**, *7* (20), 4178−4184.

(14) Treglia, A.; Ambrosio, F.; Martani, S.; Folpini, G.; Barker, A. J.; Albaqami, M. D.; De Angelis, F.; Poli, I.; Petrozza, A. Effect of Electronic Doping and Traps on Carrier Dynamics in Tin Halide Perovskites. *Mater. Horiz.* **2022**, *9* (6), 1763−1773.

(15) Dong, Y.; Zhu, W. X.; Wu, D. T.; Li, X.; Westbrook, R. J. E.; Huang, C. J.; Min, Z.; Hong, W.; Wang, B.; Min, G.; Sathasivam, S.; Palma, M.; Dimitrov, S.; Lin, C. T.; Macdonald, T. J. Crystal Growth Modulation of Tin–Lead Halide Perovskites via Chaotropic Agent. *J. Am. Chem. Soc.* **2025**, *147* (35), 31578−31590.

(16) Sanchez-Diaz, J.; Sánchez, R. S.; Masi, S.; Krecmarová, M.; Alvarez, A. O.; Barea, E. M.; Rodriguez-Romero, J.; Chirvony, V. S.; Sánchez-Royo, J. F.; Martinez-Pastor, J. P.; Mora-Seró, I. Tin Perovskite Solar Cells with >1,300 h of Operational Stability in N_2 through a Synergistic Chemical Engineering Approach. *Joule* **2022**, *6* (4), 861−883.

(17) Wu, Y.; Yuan, F.; Yang, S.; Li, E.; Wang, W.; Liu, Y.; Yang, X.; Wen, J.; Hua, L.; Yang, Y.; Lei, Y.; Chu, J.; Li, W. Tailoring Tin-Based Perovskite Crystallization via Large Cations and Pseudo-Halide Anions for High Mobility and High Stable Transistors. *Sci. Adv* **2025**, *11*, No. eadv4138.

(18) Wu, Y.; Yang, S.; Li, E.; Liu, Y.; Yuan, F.; Wen, J.; Hua, L.; Wang, W.; Yang, Y.; Lei, Y.; Chu, J.; Li, W. Low-Dimensional Templates and Delayed Crystallization for High-Quality Tin-Based Perovskite Films and High-Performance Transistors. *Nat. Commun.* **2025**, *16* (1), No. 9505.

(19) Pascual, J.; Flatken, M.; Radicchi, E.; Aldamasy, M.; Hu, S.; Solis, O. E.; Turren-Cruz, S. H.; Li, G.; Hoell, A.; Schorr, S.; Li, M.; De Angelis, F.; Musiienko, A.; Dallmann, A.; Abate, A. Unravelling the Intrinsic Reactivity and Colloidal Instability in Tin-Based Halide Perovskite Precursor Solutions. *Angew. Chem., Int. Ed.* **2026**, *65*, No. e7703450.

(20) Lanzetta, L.; Webb, T.; Zibouche, N.; Liang, X.; Ding, D.; Min, G.; Westbrook, R. J. E.; Gaggio, B.; Macdonald, T. J.; Islam, M. S.; Haque, S. A. Degradation Mechanism of Hybrid Tin-Based Perovskite Solar Cells and the Critical Role of Tin (IV) Iodide. *Nat. Commun.* **2021**, *12* (1), No. 2853.

(21) Motti, S. G.; Meggiolaro, D.; Barker, A. J.; Mosconi, E.; Perini, C. A. R.; Ball, J. M.; Gandini, M.; Kim, M.; De Angelis, F.; Petrozza, A. Controlling Competing Photochemical Reactions Stabilizes Perovskite Solar Cells. *Nat. Photonics* **2019**, *13* (8), 532−539.

(22) Alsulami, A.; Lanzetta, L.; Huerta Hernandez, L.; Rosas Villalva, D.; Sharma, A.; Gonzalez Lopez, S. P.; Emwas, A. H.; Yazmaciyan, A.; Laquai, F.; Yavuz, I.; Baran, D. Triiodide Formation Governs Oxidation Mechanism of Tin-Lead Perovskite Solar Cells via A-Site Choice. *J. Am. Chem. Soc.* **2024**, *146* (33), 22970−22981.

(23) Diaz-Perez, T.; Pareja-Rivera, C.; Pascual, J.; S.H. J.; Masi, S.; Barea, E. M.; Turren-Cruz, S. H.; Mora-Seró, I. The Dual Role of Borohydride Salts in Enhancing Perovskite Solar Cell Performance and Stability. *Sustainable Energy Fuels* **2026**, *10* (4), 1069-1079.

(24) Macdonald, T. J.; Lanzetta, L.; Liang, X.; Ding, D.; Haque, S. A. Engineering Stable Lead-Free Tin Halide Perovskite Solar Cells: Lessons from Materials Chemistry. *Adv. Mater.* **2023**, *35*, No. 2206684.

(25) Li, B.; Chang, B.; Pan, L.; Li, Z.; Fu, L.; He, Z.; Yin, L. Tin-Based Defects and Passivation Strategies in Tin-Related Perovskite Solar Cells. *ACS Energy Lett.* **2020**, *5* (12), 3752−3772.

(26) Finkelstein, D. A.; Jones, D. J.; Hernandez-Burgos, K.; Abruña, H. D. Electro-Oxidation of BH4- in Dimethylsulfoxide and Dimethylformamide Studied by Rotating Disk Electrode Voltammetry. *J. Power Sources* **2011**, *196* (15), 6223−6227.

(27) DeQuilettes, D. W.; Vorpahl, S. M.; Stranks, S. D.; Nagaoka, H.; Eperon, G. E.; Ziffer, M. E.; Snaith, H. J.; Ginger, D. S. Impact of Microstructure on Local Carrier Lifetime in Perovskite Solar Cells. *Science* **2015**, *348* (6235), 683−686.

(28) Taddei, M.; Smith, J. A.; Gallant, B. M.; Zhou, S.; Westbrook, R. J. E.; Shi, Y.; Wang, J.; Drysdale, J. N.; McCarthy, D. P.; Barlow, S.; Marder, S. R.; Snaith, H. J.; Ginger, D. S. Ethylenediamine Addition Improves Performance and Suppresses Phase Instabilities in Mixed-Halide Perovskites. *ACS Energy Lett.* **2022**, *7* (12), 4265−4273.

(29) Min, G.; Westbrook, R. J. E.; Jiang, M.; Taddei, M.; Li, A.; Webb, T.; Sathasivam, S.; Azaden, A.; Palgrave, R. G.; Ginger, D. S.; Macdonald, T. J.; Haque, S. A. The Effect of Antisolvent Treatment on the Growth of 2D/3D Tin Perovskite Films for Solar Cells. *ACS Energy Lett.* **2025**, *10* (1), 254−262.
(30) Pothoof, J.; Westbrook, R. J. E.; Giridharagopal, R.; Breshears, M. D.; Ginger, D. S. Surface Passivation Suppresses Local Ion Motion in Halide Perovskites. *J. Phys. Chem. Lett.* **2023**, *14*, 6092−6098.
(31) Taddei, M.; Contreras, H.; Doan, H. N.; McCarthy, D. P.; Seo, S.; Westbrook, R. J. E.; Graham, D. J.; Datta, K.; Carroy, P.; Muñoz, D.; Correa-Baena, J. P.; Barlow, S.; Marder, S. R.; Smith, J. A.; Snaith, H. J.; Ginger, D. S. Diamine Surface Passivation and Postannealing Enhance the Performance of Silicon-Perovskite Tandem Solar Cells. *ACS Appl. Mater. Interfaces* **2025**, *17* (26), 38754−38762.

https://doi.org/10.1021/acsenergylett.6c01751
ACS Energy Lett. XXXX, XXX, XXX−XXX